MNRAS **000**, 1–10 (2018) Preprint 10 March 2024 Compiled using MNRAS LATEX style file v3.0

Investigating the origin of the faint non-thermal emission of the Arches cluster using the 2015-2016 *NuSTAR* and *XMM–Newton* X-ray observations

Ekaterina Kuznetsova,[1]★ Roman Krivonos,[1] Maïca Clavel,[2] Alexander Lutovinov,[1,3] Dmitry Chernyshov,[4] JaeSub Hong,[5] Kaya Mori,[6] Gabriele Ponti,[7] John Tomsick,[8] Shuo Zhang[9]

[1] *Space Research Institute of the Russian Academy of Sciences, Profsoyuznaya 84/32, 117997 Moscow, Russia*
[2] *Univ. Grenoble Alpes, CNRS, IPAG, F38000 Grenoble, France*
[3] *Higher School of Economics, Myasnitskaya 20, 101000 Moscow, Russia*
[4] *I.E. Tamm Theoretical Physics Division of P.N. Lebedev Institute of Physics, Leninskii pr. 53, 119991 Moscow, Russia*
[5] *Harvard-Smithsonian Center for Astrophysics, 60 Garden St., Cambridge, MA 02138, USA*
[6] *Columbia Astrophysics Laboratory, Columbia University, New York, NY 10027, USA*
[7] *Max-Planck-Institut für extraterrestrische Physik, Giessenbachstrasse 1, Garching, 85748, Germany*
[8] *Space Sciences Laboratory, University of California, 7 Gauss Way, Berkeley, CA 94720-7450, USA*
[9] *MIT Kavli Institute, 77 Massachusetts Ave, Cambridge, MA 02139 USA*

arXiv:1901.03121v1 [astro-ph.HE] 10 Jan 2019

Accepted XXX. Received YYY; in original form ZZZ

ABSTRACT

Recent *NuSTAR* and *XMM–Newton* observations of the molecular cloud around the Arches stellar cluster demonstrate a dramatic change both in morphology and intensity of its non-thermal X-ray emission, similar to that observed in many molecular clouds of the Central Molecular Zone at the Galactic Center. These variations trace the propagation of illuminating fronts, presumably induced by past flaring activities of Sgr A★. In this paper we present results of a long *NuSTAR* observation of the Arches complex in 2016, taken a year after the previous *XMM+NuSTAR* observations which revealed a strong decline in the cloud emission. The 2016 *NuSTAR* observation shows that both the non-thermal continuum emission and the Fe K_α 6.4 keV line flux are consistent with the level measured in 2015. No significant variation has been detected in both spectral shape and Fe K_α equivalent width $EW_{6.4\ \mathrm{keV}}$, which may be interpreted as the intensity of the Arches non-thermal emission reaching its stationary level. At the same time, the measured 2016 non-thermal flux is not formally in disagreement with the declining trend observed in 2007-2015. Thus, we cannot assess whether the non-thermal emission has reached a stationary level in 2016, and new observations, separated by a longer time period, are needed to draw stringent conclusions. Detailed spectral analysis of three bright clumps of the Arches molecular cloud performed for the first time showed different $EW_{6.4\ \mathrm{keV}}$ and absorption. This is a strong hint that the X-ray emission from the molecular cloud is a mix of two components with different origins.

Key words: ISM: clouds, X-rays: individual (Arches cluster)

1 INTRODUCTION

The Arches cluster (Cotera et al. 1996; Serabyn et al. 1998) is a massive star cluster, which is located in the Galactic Center (GC) region at the projected angular distance of 28 pc from Sgr A★. The cluster contains more than 160 O-type stars with initial masses larger than 20 $M_\odot$ and its average mass density is $\sim 3\times10^5\ M_\odot \mathrm{pc}^{-3}$ (Figer et al. 1999, 2002). The Arches core is about 9″ (~ 0.35 pc at 8 kpc) in radius (Figer et al. 1999).

The first X-ray observation of the region around the Arches cluster with *Chandra* (Yusef-Zadeh et al. 2002) re-

★ E-mail: eakuznetsova@cosmos.ru

© 2018 The Authors

vealed its bright X-ray emission. This emission, characterized by the 6.7 keV Fe line, was detected in the narrow region consistent with the Arches cluster position (hereafter "the core"). The thermal emission of the cluster was attributed to the multiple collisions between strong winds of massive stars (Yusef-Zadeh et al. 2002; Wang et al. 2006; Capelli et al. 2011a). In addition to the cluster's core emission, the extended emission of a different origin, spatially consistent with a nearby molecular cloud, was detected around the cluster (hereafter "the cloud"). The observed prominent Fe K_α line and the power-law continuum emission point out to its non-thermal nature. (Wang et al. 2006; Tsujimoto et al. 2007; Capelli et al. 2011b; Tatischeff et al. 2012; Krivonos et al. 2014, 2017; Clavel et al. 2014).

Two main hypotheses have been developed to explain the non-thermal emission from the Arches "cloud" emission. The first approach implies irradiation of the molecular cloud by an external X-ray source. The possible X-ray sources inside or nearby the cloud have been excluded, based on the required X-ray luminosity (Capelli et al. 2011b) to explain the 6.4 keV line flux (Tatischeff et al. 2012; Krivonos et al. 2014). The sufficient luminosity could be provided by a nearby X-ray source, e.g. 1E1740.7–2942 (Churazov et al. 1993) or with the past activity of Sgr A*, as originally suggested by Sunyaev et al. (1993) to explain the fluorescent line emission observed in the giant molecular cloud Sgr B2 in the GC region (see also Koyama et al. 1996; Sunyaev & Churazov 1998; Murakami et al. 2000; Revnivtsev et al. 2004; Terrier et al. 2010; Zhang et al. 2015). The hypothesis of the past Sgr A*'s flaring activity is also supported by the discovery of a propagation of Fe K echos in the Central Molecular Zone (CMZ), where Sgr A* is presumably the source of the illumination on the clouds (Ponti et al. 2010, 2013; Clavel et al. 2013; Ryu et al. 2013; Churazov et al. 2017a,b; Terrier et al. 2018).

Alternatively, a fluorescent emission of the molecular cloud can be a result of bombardment by low-energy cosmic ray (CR) particles (Capelli et al. 2011b; Tatischeff et al. 2012). The steady non-thermal continuum and Fe Kα flux observed in the Arches cloud for a decade was initially considered as a strong evidence for the CR heating of the Arches molecular cloud (Tatischeff et al. 2012). However, a recently discovered time variability of the non-thermal power-law continuum and 6.4 keV line (Clavel et al. 2014), strongly contradicts the CR scenario (see e.g. Dogiel et al. 2014) for a significant fraction of this emission.

Using the 2015 *XMM+NuSTAR* data set, Krivonos et al. (2017) showed that the Arches cloud experienced a strong emission decrease, along with a significant decrease of the Fe K_α equivalent width (EW). This could indicate either a change in the reflection geometry (illumination of different structures along the line of sight) or that the putative CR component has become more dominant. In any case, the question remains whether the non-thermal continuum and the 6.4 keV line emission will decrease to a zero flux level when the X-ray illuminating front leaves the molecular cloud or if some background CR heating takes place.

As discussed above, the variable component of the Arches complex non-thermal emission is generated by Thomson scattering of X-ray flare photons leaving the Arches cloud complex. Chernyshov et al. (2018) suggested that the other (possibly stationary) component can be caused by either i) Thompson scattering of photons from the same or a different X-ray flare, ii) another molecular cloud complex which is situated at large distance from the Arches cluster and on the same line of sight, or iii) the excitation of CR particles, however more restrictions must be satisfied. The authors argue that in case of a single cloud complex (i) the *EW* variations are likely associated with iron abundance changes in it during the flare moving across the cloud. For the second case with two different clouds (ii), Chernyshov et al. (2018) calculated the temporal delay of the Compton echo for the first variable component at about 100 yrs. This is in agreement with Churazov et al. (2017a) who estimated X-ray flare event with 110 yrs age. For the second variable component the estimated time delay is about 230 yrs (Chernyshov et al. 2018). It is more likely that these two components were caused by the different flares rather than the same flare. The suggestion of two different flares are consistent with scenario of two flares of Sgr A* 110 and 240 yrs ago (Clavel et al. 2013; Terrier et al. 2018; Chuard et al. 2018).

Changes in the morphology of the Arches cluster cloud are similar to those seen for Sgr B2, where the non-thermal emission likely reaching the background level as well, revealing a substructure of two compact cores and a newly emerging cloud that confirms the propagation of the illuminating front(s) from an X-ray flare (Zhang et al. 2015). These similarities between the Arches cloud emission and GC molecular clouds (Krivonos et al. 2017) support the reflection mechanism of the non-thermal emission.

In this work we analyzed observations of the Arches cluster region with *NuSTAR* in 2015-2016 and *XMM–Newton* in 2015, with the aim to monitor the non-thermal emission around the cluster. Additionally, we carried out detailed spectral analysis of the emission clumps detected with *XMM–Newton* observations in 2015. The paper is structured as follows: in Sect. 2 we describe observations of the Arches cluster with *NuSTAR* in 2016 and outline the data analysis; 2016 *NuSTAR* data analysis morphology and spectral analyses are presented in Sect. 3; Sect. 4 contains the analysis of the combined *NuSTAR* and *XMM–Newton* 2015-2016 observations. We investigate the substructure of the Arches cloud non-thermal emission revealed by the 6.4 keV line emission clumps observed with *XMM–Newton* (Sect. 5). We discuss and summarize the obtained results in Sect. 6.

2 OBSERVATION AND DATA ANALYSIS

The Arches cluster region was observed in October 2016 during the *NuSTAR* Legacy survey[1] of the Sgr A molecular clouds with a total exposure time of 150 ks. The list of the used *NuSTAR* observations is shown in Table 1.

The hard X-ray orbital telescope *NuSTAR* (Harrison et al. 2013), launched in 2012, provides imaging at energies above 10 keV with sub-arcminute angular resolution. *NuSTAR* carries two identical co-aligned X-ray telescope modules (referred as FPMA and FPMB) with a full width at half maximum (FWHM) of 18″. The energy

[1] https://www.nustar.caltech.edu/page/legacy_surveys

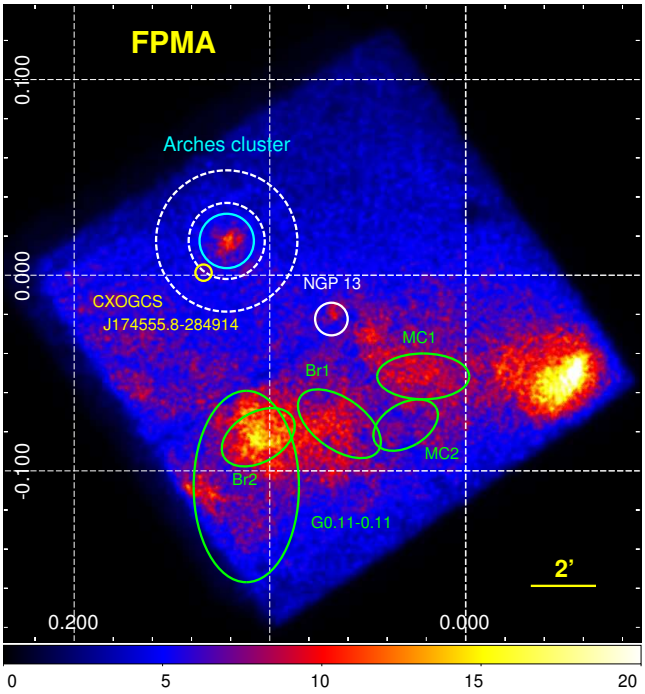


Figure 1. *NuSTAR* 3 – 79 keV image in Galactic coordinates of Sgr A molecular clouds region, including the Arches cluster, taken in 2016 (FPMA data only, exposure 150 ks). The extraction of the source and background spectra was done, respectively, in the circle $R = 50''$ and annulus ($70'' < R < 130''$). Solid elliptical sky regions shows positions of selected Sgr A molecular clouds (Clavel et al. 2013). NGP 13 label denotes position of a hard X-ray source detected in the *NuSTAR* survey of the GC region (Hong et al. 2016). Small solid circle labeled CXOGCS J174555.8–284914 shows the position of corresponding X-ray source (Sect. 4.1). The image was smoothed using DMIMGADAPT task from CIAO-V.4.9 with the following parameters: tophat kernel, smoothing scales 1 – 20, the number of scales is 30, the minimum number of counts is 20.

Table 1. The list of the Arches cluster observations, which have been used in this work.

Experiment	ObsID	Start Date	Exposure, s
XMM	0762250301	2015-09-27 15:48:39	114000
NuSTAR	40101001002	2015-10-19 06:21:08	107189
	40101001004	2015-10-25 13:56:08	107856
	40202001002	2016-10-28 13:16:08	150856

response covers a wide range from 3 to 79 keV with a spectral resolution of 400 eV (FWHM) at 10 keV.

Due to *NuSTAR*'s known 'stray-light' issue, when detectors can be illuminated by X-rays passing outside the field of view the X-ray optics (Madsen et al. 2017), the data from FPMB are strongly contaminated by photons from the bright X-ray source GX 3+1, which forced us to exclude FPMB data in this work. Fig. 1 shows the FPMA image of the Arches cluster region in the full 3 – 79 keV energy band. Arches was observed at $\sim 4'$ distance from the optical axis, which led to a somewhat efficiency decrease, however without a visible distortion of the point spread function (PSF).

It is worth noting that celestial coordinates of each photon registered by *NuSTAR* are subject to a systematic offset, which can be as high as $14''$ (Mori et al. 2015). We noticed an offset between the cluster's centroid position and its catalogued coordinates at the level of $3 - 4''$. Similar to Krivonos et al. (2017), we performed an astrometric correction by shifting coordinates of each photon using a reference position of the Arches core centroid, measured in the first *NuSTAR* observation of the Arches cluster in 2012 (Krivonos et al. 2014), when the offset was negligible.

We extracted spectrum of the Arches cluster complex, and corresponding response matrices, using the *nuproducts* task, a part of *NuSTAR* Data Analysis Software package (NUSTARDAS V.1.8.0), built in HEASOFT software (version 6.22). Note that in this paper we often compare our results with those of Krivonos et al. (2017) who used older HEASOFT version 6.17. We checked that different versions do not introduce strong deviations to the results. The source extraction region was a circle with a radius of $50''$ positioned at the cluster position $R.A. = 17^h45^m50.52^s$, $Dec. = -28°49'22.41''$ (Krivonos et al. 2014, 2017). The background spectrum was obtained from the annulus region within the radii range $R = 70 - 130''$ (see Fig. 1), excluding $R = 15''$ circular region of the source CXOGCS J174555.8–284914 (Law & Yusef-Zadeh 2004), as described in Sect. 4.1. The interactive spectral and 2D image analysis were done using XSPEC (Arnaud 1996) and SHERPA (Freeman et al. 2001) tools included, respectively, in HEASOFT 6.22 and CIAO-V.4.9 (Fruscione et al. 2006) software packages.

3 *NuSTAR* OBSERVATIONS OF THE ARCHES CLUSTER IN 2016

3.1 2D image analysis

Since the Arches cluster demonstrated a strong drop of its non-thermal emission in 2007-2015 (Clavel et al. 2014; Krivonos et al. 2017), one would expect a further fall even below the detection threshold. The main question we address in this section is whether the Arches stellar cluster is still surrounded by the spatially extended emission, previously detected with *NuSTAR* in 2012-2015 (Krivonos et al. 2014, 2017). The *NuSTAR* angular resolution of $18''$ (FWHM) does not allow us to directly resolved the emission around the cluster's core. Therefore we use a simple 2D image analysis with the SHERPA package to estimate a spatial extension of the cluster emission compared to that expected from the *NuSTAR* PSF. SHERPA performs spatial fitting of a data image using a 2D source model convolved with supplied instrumental PSF.

We first analyzed the 2016 *NuSTAR* 3 – 79 keV image of the Arches cluster region using 2D Gaussian model `G1` with a fixed $4''$ FWHM (PSF smearing effect) and free center position, representing a point-like X-ray source. The model is represented in the SHERPA notation as `psf(gauss2d.G1)*emap+const2d.bkg*emap`, where `G1` is 2D Gaussian, associated with the emission of the stellar cluster, `emap` contains exposure map, and `const2d.bkg` component estimates the background count rate, in the assumption of

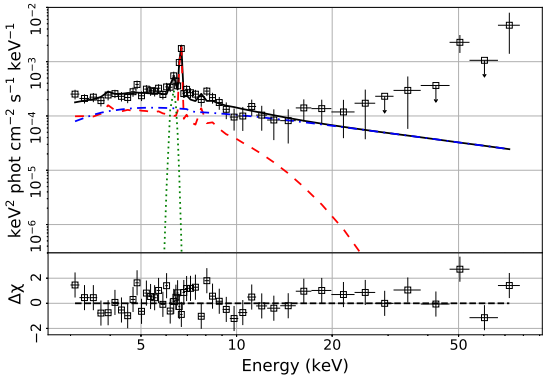


Figure 2. The Arches cluster *NuSTAR* 2016 spectrum extracted from the 50″ circle region around the cluster (detector module A only). Solid, dashed, dotted and dash-dotted lines are the total model (see Table 2), thermal *APEC*, Fe K_α line and non-thermal power-law components respectively.

a flat distribution. As shown in Fig. 1, the fitting area was limited by a circle with $R = 50''$ around the cluster's centroid position and the background count rate was estimated in the annulus $70'' < R < 130''$ with the same center position, excluding the circle region with $R = 15''$ of X-ray source CXOGCS J174555.8–284914 (Sect. 4.1). The difference between the 3 – 79 keV image and the best-fit model is characterized by strong deviations indicating that the X-ray emission of the Arches cluster is not consistent with a point-like X-ray source (Wang et al. 2006; Law & Yusef-Zadeh 2004). To quantitatively estimate the spatial scale of the extended emission of the Arches cluster we added a second 2D Gaussian model `G2` with a free position and FWHM parameter. The list of free parameters of this new complex model includes the position of `G1`, the position and width of `G2`, and the flat background level. The extended model provides a good fit to the data, characterized by no strong deviations in the residuals, and fit statistics $\chi^2_r \approx 1$. The fitting procedure estimates a spatial scale of the extended emission `G2` as being $32'' \pm 7''$ FWHM, which is significantly larger than the *NuSTAR* PSF (18″ FWHM). This result indicates that the spatially extended emission of the Arches cluster is still present in 2016. The position of the `G2` extended component is shifted off by $13'' \pm 3''$ from the position of the Arches stellar core (`G1`), which also indicates that the extended emission is not associated with the stellar cluster.

3.2 Spectral analysis

As shown in the previous subsection, the extended emission, associated with the non-thermal radiation of the neutral or low ionization state material of the molecular cloud is still present around the stellar cluster. For quantitative evaluation, we perform a spectral analysis comparing the recent 2016 *NuSTAR* observations with previous results from by Krivonos et al. (2017) based on the *NuSTAR* and *XMM–Newton* data acquired in 2015.

We reduced the 2016 *NuSTAR* observation of the Arches cluster and extracted source and background spectra from 50″ circular and 70 – 130″ annulus regions, respectively, as described in Section 2. The background-subtracted FPMA spectrum of the Arches cluster region is shown in Fig. 2. To fit the spectrum, we applied the same spectral model *wabs* × (*APEC* + *Gaussian* + *powerlaw*) used in Krivonos et al. (2017), which contains the thermal emission of the stellar cluster described by the collisionally ionized plasma emission model (*APEC*) and the non-thermal emission of the molecular cloud in the form of power-law and Gaussian 6.4 keV line. The thermal emission is characterized by kT, $Z/Z_\odot$, and I_{kT} parameters describing, respectively, the temperature in keV, the metallicity relative to the solar one, and the normalization in units of $10^{-18} \int n_e n_H dV/(4\pi D^2)$, where n_e and n_H are the electron and proton number densities in units of cm^{-3}, and D is the cluster distance in cm. The metallicity was fixed at $Z = 1.7Z_\odot$ according to Tatischeff et al. (2012). The non-thermal emission is approximated by a power-law continuum and Fe 6.4 keV line, represented by a Gaussian with the width fixed at 0.1 keV. All the emission spectral components are subject to interstellar photo-electric absorption modeled with *wabs* in XSPEC. Due to limited energy response of the *NuSTAR* below 5 keV, the fitting procedure does not allow us to constrain the absorption, and we fixed it at $N_H = 9.5{\times}10^{22}$ cm^{-2} (Tatischeff et al. 2012). The equivalent width (EW) of the 6.4 keV line was estimated with the SHERPA package with respect to the *powerlaw* component only. The fitting procedure demonstrated a strong correlation between components, causing a degeneracy of model parameters: plasma temperature kT and power-law photon index Γ. To overcome this, for the following analysis we fixed the *APEC* temperature at 2.4 keV, as measured by Krivonos et al. (2017) in 2015 *NuSTAR* observations. Best-fitting model parameters are listed in Table 2. For comparison with 2015 *NuSTAR* observations we included to the table the best-fitting parameters of the same model adopted from Krivonos et al. (2017).

The spectral analysis of the *NuSTAR* observations of the Arches cluster complex in 2015 and 2016 does not demonstrate strong variations of both thermal emission of the cluster and non-thermal emission of the surrounding molecular cloud. The main parameters of the non-thermal emission, power-law slope and normalization, and *EW* of the iron 6.4 keV line, are consistent within uncertainties between the observations. We conclude that further observations of the Arches cluster region are needed to confirm or deny the stationary level of the Arches cloud non-thermal emission.

4 THE COMBINED 2015-2016 DATA SET

4.1 2D image analysis

Assuming that the morphology of the Arches extended emission has not significantly changed since 2015 (which is confirmed by spectral analysis, see previous section), we combined the *NuSTAR* observations from 2015 and 2016 into one data set, producing mosaic images in three energy bands: 3 – 79 keV, 3 – 10 keV and 10 – 20 keV, shown in Fig. 3. The full 3 – 79 keV band mosaic image reveals both the emission of the stellar cluster and the extended emission. The surface brightness distribution of the Arches in the 3–10 keV band is dominated by the stellar cluster. Finally, the hard 10–20 keV

Table 2. Best-fit model parameters for the Arches cluster region, measured with *NuSTAR* in 2015 (Krivonos et al. 2017) and 2016 (this work). Model: $wabs \times (APEC + Gaussian + powerlaw)$.

Parameter	Unit	2015 yr	2016 yr	2015&2016
$N_{\rm H}$	10^{22} cm^{-2}	9.5 (fixed)	9.5 (fixed)	9.5 (fixed)
kT	keV	$2.4^{+1.5}_{-0.4}$	2.4 (fixed)	2.4 (fixed)
$I_{\rm kT}$	see Sect. 3.2	9.2 ± 5.3	$8.4^{+2.1}_{-4.4}$	$9.1^{+1.2}_{-1.4}$
$\Delta E_{6.4\ \rm keV}$	keV	0.1 (fixed)	0.1 (fixed)	0.1 (fixed)
$E_{6.4\ \rm keV}$	keV	6.3 ± 1.1	6.3 ± 0.3	6.3 ± 0.1
$F_{6.4\ \rm keV}$	10^{-6} ph cm^{-2} s^{-1}	2.6 ± 1.5	$2.5^{+3.1}_{-1.7}$	2.4 ± 1.2
$EW_{6.4\ \rm keV}$	eV	450 ± 150	580 ± 250	540 ± 140
Γ		$2.4^{+0.6}_{-0.3}$	$2.7^{+0.4}_{-0.5}$	2.6 ± 0.2
$F^{\rm pow}_{3-20\ \rm keV}$	10^{-13} erg cm^{-2} s^{-1}	$5.6^{+1.2}_{-0.9}$	$4.4^{+2.1}_{-3.1}$	5.8 ± 0.8
$\chi^2_{\rm r}$/d.o.f.		0.97/364	0.82/204	0.91/574

Table 3. The 2D-fitting procedure best-fit parameters with the 1σ errors of the $50''$ central region of the Arches cluster for the $3-79$, $3-10$ and $10-20$ keV energy bands, based on 2015-2016 data.

Parameter	$3-79$ keV	$3-10$ keV	$10-20$ keV
Core (2D Gaussian, G1)			
Center RA (J2000)	17:45:50.52	17:45:50.54	
Center Dec (J2000)	-28:49:22.39	-28:49:22.35	
FWHM	$4''$ (fixed)	$4''$ (fixed)	
Norm. ($\times 10^{-3}$)	3.7±0.5	3.6±0.5	
Cloud (2D Gaussian, G2)			
Center RA (J2000)	17:45:51.47	17:45:51.35	17:45:52.05
Center Dec (J2000)	-28:49:30.76	-28:49:29.71	-28:49:31.72
FWHM	$41''.9 \pm 3''.5$	$37''.5 \pm 3''.5$	$61''.0^{+14.1}_{-10.0}$
Norm. ($\times 10^{-6}$)	63.8±11.8	67.0±15.2	$6.1^{+1.7}_{-1.3}$

band highlights the distribution of the non-thermal emission around the Arches cluster.

We then repeated the 2D image analysis on the combined *NuSTAR* mosaic images, in order to better determine properties of the extended emission. The best-fit model and residuals of the fit for $3-79$ keV energy band image are shown in Fig 4. The residual image shows small scale fluctuations with amplitude an order of magnitude less than the input $3-79$ keV *NuSTAR* mosaic image. The positions of the residual fluctuations are spatially consistent with the 6.4 keV Arches cloud clumps described in Sect. 5. Note that we excluded the G1 Gaussian model from the fitting procedure in the $10-20$ keV band due to negligible contribution of the thermal emission from the stellar cluster at energies above 10 keV. The best-fitting model parameters are shown in Table 3. In all three bands the spatial size of the G2 component is larger than the *NuSTAR* PSF, which confirms the presence of the extended emission around the cluster above 10 keV. We checked that the centroid position of the extended G2 component in the $3-10$ keV and $10-20$ keV bands are consistent with each other within 3σ confidence interval, which points out to the same extended component detected in the soft and the hard energy bands, respectively.

Note the G2 component is more extended in the $10-20$ keV band compared to the $3-10$ keV (see Table 3). This is mainly caused by lower statistics of the Arches non-thermal emission above 10 keV and nearby image fluctuations probably associated with the systematic noise. To estimate the level of the systematics we analyzed the source-free region of the $10-20$ keV image and found that the relative non-statistical fluctuations can be as high as $\sim 15\%$.

Fig. 3 also reveals an X-ray excess located $\sim 1'$ to the east of the cluster, clearly seen in the full $3-79$ keV and hard $10-20$ keV band images. Its centroid position $R.A. = 17^h45^m56.0^s$, $Dec. = -28°49'16.4''$ is consistent within 3σ uncertainty with the position of the X-ray source CXOGCS J174555.8–284914 (Yusef-Zadeh et al. 2002; Law & Yusef-Zadeh 2004), as identified with the SIMBAD astronomical database (Wenger et al. 2000). The source, also labeled as A4 in Yusef-Zadeh et al. (2002), is highly absorbed ($N_{\rm H} \sim 4 \times 10^{23}\ cm^{-2}$) and has a hard power-law like spectrum with a peak near the 6.4 keV Fe line (Law & Yusef-Zadeh 2004). To avoid a possible contribution from this source to the background count rate assessment, we excluded $15''$ circular region around it from the spatial and spectral analysis.

4.2 Spectral analysis

To better estimate the model parameters, we simultaneously fitted the 2015 and 2016 data sets for the following spectral analysis. The last column of Table 2 shows the results of the fitting procedure with the same model used in Sect. 3.2, and Fig. 5 demonstrates the combined spectral fit. The best-fitting model parameters of the data sets are in general agreement with individual *NuSTAR* observations in 2015 and 2016.

To extend a spectral coverage to the low energies, and to determine the total line-of-sight absorption column density $N_{\rm H}$, we added spectrum based on *XMM–Newton* observation carried out on 27$^{\rm th}$ September 2015 (Table 1), extracted from the same $50''$ circular region (Krivonos et al. 2017).

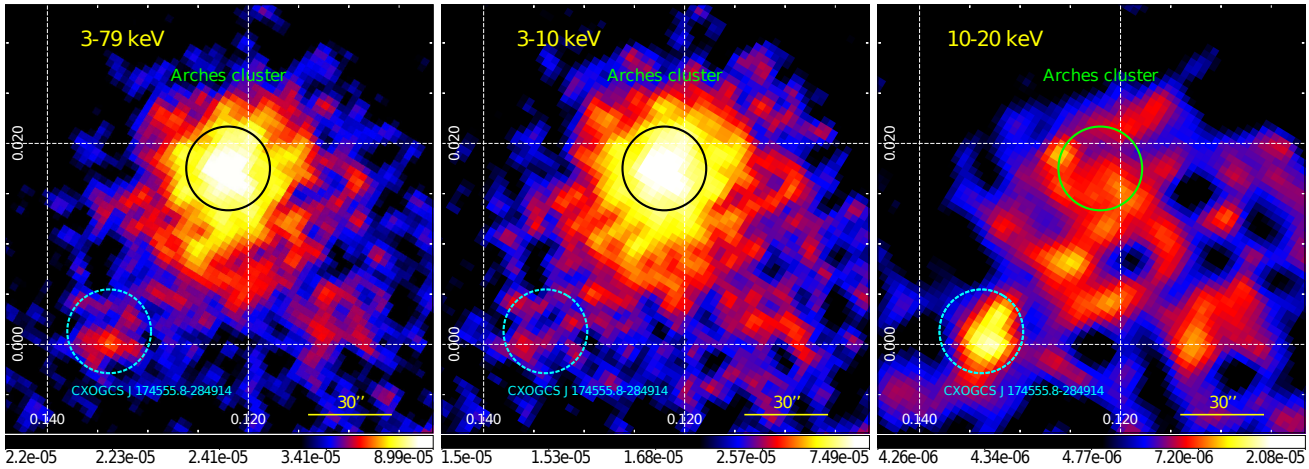


Figure 3. The *NuSTAR* mosaic images of the Arches cluster region 2015-2016 in 3 – 79 keV (left), 3 – 10 keV (center) and 10 – 20 keV (right) energy bands. The images are corrected for the exposure and adaptively smoothed with *dmimgadapt* task from CIAO-V.4.9 using a tophat kernel with parameters as for Fig. 1. The sky grid indicates Galactic coordinates in degrees. The solid circle with the radius of 15″ shows the position of the Arches stellar cluster. The 15″ dashed circle denotes the position of the hard X-ray point source CXOGCS J174555.8–284914.

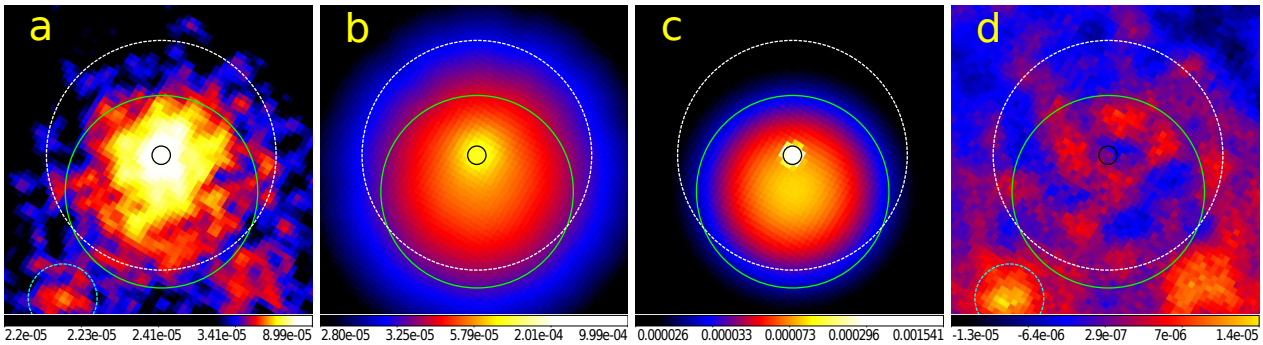


Figure 4. An example of 2D fitting procedure of the Arches cluster mosaic image. Small and large solid regions are `G1` and `G2` components of the best-fit Gaussian model with central positions and FWHM radii listed in Table 3, respectively. The fitting area constrained by the $R = 50''$ circle region (large dashed circle) with excluded $R = 15''$ region of the source CXOGCS J174555.8–284914 (small dashed circle). a) The 3 – 79 keV *NuSTAR* mosaic image. b) The Best-fit spatial model of the Arches cluster complex in 3 – 79 keV energy band with two gaussians `G1` and `G2` convolved with the NuSTAR PSF. c) The same as plot b, but not convolved with the PSF. d) The residuals after subtracting best-fitting model smoothed with a tophat kernel ($R = 3$ px).

The combined 2015 *XMM–Newton* and 2015-2016 *NuSTAR* broad-band spectrum of the Arches cluster region is shown in Fig. 6. The best-fitting model parameters with the free absorption parameter are listed in Table 4. The $N_{\rm H}$ value was determined as $(9.3 \pm 0.5) \times 10^{22}$ cm^{-2}, which is consistent with $N_{\rm H} = (9.5 \pm 0.3) \times 10^{22}$ cm^{-2} measured by Tatischeff et al. (2012). The joint fit gives a solid measurement of the power-law $\Gamma = 2.21 \pm 0.15$ up to 30 – 40 keV, which is in agreement within 1σ uncertainty with $\Gamma = 2.03 \pm 0.16$ measured by Krivonos et al. (2017).

To describe the Arches non-thermal continuum in the combined 2015 *XMM–Newton* and *NuSTAR* spectrum, additionally to a simple power-law model, Krivonos et al. (2017) also applied CR-induced emission model developed by Tatischeff et al. (2012) and self-consistent X-ray reflection model REFLIONX (Ross & Fabian 2005). We checked that adding 2016 *NuSTAR* data set to the joint 2015 *XMM–Newton* and *NuSTAR* fit allows to better constrain the parameters of these models, however, the improvements are still not enough to significantly confirm or rule out either of them. For simplicity we do not list the best-fitting results of physically motivated spectral models in this paper.

5 6.4 KEV CLUMPS OF THE ARCHES CLOUD

The broad-band *NuSTAR* spectral analysis of the Arches non-thermal X-ray emission has been previously performed in a wide circular region covering the stellar cluster itself and surrounding molecular cloud (see Sections 3 and 4, Krivonos et al. 2014, 2017, and). Other studies, mainly based on *XMM–Newton* observations, used an elliptical region excluding the stellar cluster (see ellipse parameters in Tatischeff et al. 2012; Clavel et al. 2014; Krivonos et al. 2017). Thus, the spectral extraction region often included the whole Arches non-thermal emission, which was characterized by regular and extended shape, traced by iron 6.4 keV line flux (Tatischeff et al. 2012). Note that integrating the signal over large region may average emission having different trend and/or different origin (see e.g. Clavel et al.

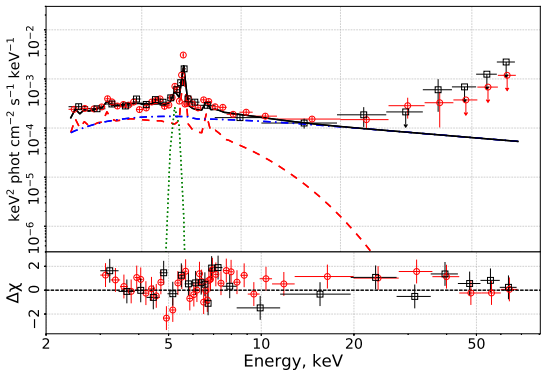


Figure 5. Joint 2015-2016 *NuSTAR* X-ray spectrum of the Arches cluster region. 2015 and 2016 *NuSTAR* data are marked with circles and squares, respectively. The total model is represented by a solid line. Dashed, dotted and dash-dotted lines represent thermal plasma, 6.4 keV emission line (width fixed at 0.1 keV) and power-law continuum model components, respectively.

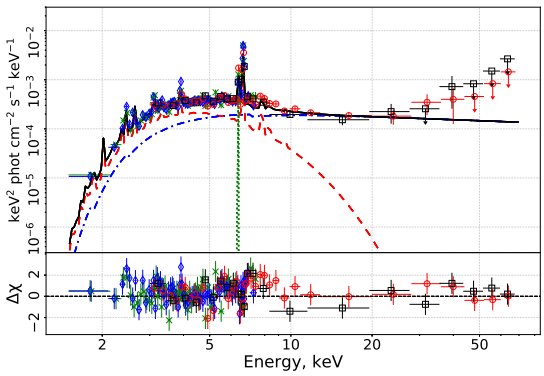


Figure 6. Joint *XMM–Newton* 2015 and *NuSTAR* 2015-2016 spectrum of the Arches cluster extracted from the 50″ circle region around the stellar cluster. Crosses and diamonds represent MOS1/MOS2 and PN data, respectively. Circles and squares show, respectively, 2015 and 2016 *NuSTAR*/FPMA data. The best-fitting spectral model (solid line, Table 4) includes emission of the thermal plasma (dashed), fluorescent Fe Kα line emission (dotted) with a fixed width of 0.01 keV and power-law continuum (dash-dotted).

2013). The smaller ellipse which was used in the previous *XMM–Newton* analysis may still be too large to understand the complexity of the current *EW* variation. To investigate this we carried out new analysis of the clumps revealed in the 6.4 keV line using the 2015 *XMM–Newton* data.

We followed the procedure described in Krivonos et al. (2017) for analyzing the *XMM–Newton* MOS1, MOS2 and PN data and extracted 2 – 7.5 keV spectra of three clumps S, N and E (see Fig. 7) within elliptical regions, which parameters are listed in Table 5. The regions are shown in Fig. 7. Note that for the clump N region we excluded the elliptical region containing the bright 6.7 keV line emission from the Arches cluster core. The spectra of clumps are

Table 4. Best-fit parameters for the Arches cluster extracted from $R = 50''$ circular region, based on 2015 *XMM–Newton* and 2015-2016 *NuSTAR* observations. For comparison observations are shown best-fit parameters of the 2015 *NuSTAR*+XMM data (Krivonos et al. 2017). Model: $wabs \times (APEC + Gaussian + powerlaw)$.

Parameter	Unit	2015	2015+2016
$N_{\rm H}$	10^{22} cm^{-2}	$9.3^{+0.9}_{-0.5}$	9.3 ± 0.5
kT	keV	1.95 ± 0.14	$1.95^{+0.16}_{-0.12}$
$I_{\rm kT}$	see Sect. 3.2	18 ± 3	17 ± 3
$\Delta E_{6.4\ \rm keV}$	keV	0.01 (fixed)	0.01 (fixed)
$E_{6.4\ \rm keV}$	keV	6.38 ± 0.02	6.38 ± 0.03
$F_{6.4\ \rm keV}$	10^{-6} ph cm^{-2} s^{-1}	3.1 ± 0.6	3.0 ± 0.6
$EW_{6.4\ \rm keV}$	eV	700^{+100}_{-90}	660 ± 80
Γ		2.03 ± 0.16	2.21 ± 0.15
$I_{\rm pow}$	10^{-5} cm^{-2} s^{-1} keV^{-1}	22^{+10}_{-7}	33^{+13}_{-9}
C		0.82 ± 0.04	0.69 ± 0.04
$\chi^2_{\rm r}$/d.o.f.		1.00/918	0.97/1167

shown in Fig. 8. Each spectrum was approximated with the XSPEC model $wabs \times (APEC + Gaussian^{2.45\ \rm keV} + powerlaw) + Gaussian^{6.4\ \rm keV}$, consistent with previous *XMM–Newton* study of the Arches non-thermal emission by Clavel et al. (2014). The spectral model includes the APEC thermal emission of the astrophysical plasma with $kT = 2.2$ keV (chosen to mimic the combination of 1 and 7 keV plasma components in the Galactic center, Clavel et al. 2014), non-thermal power-law continuum with a fixed photon index $\Gamma = 1.6$ and unabsorbed Fe K_α 6.4 keV line with a fixed width of 0.01 keV. Following Krivonos et al. (2017) we also added an absorbed Gaussian line at 2.45 keV, presumably belonging to the K_α line from He-like Sulfur (S). The strength of photo-electric absorption is freely fitted for each clump individually. The equivalent width of the Gaussian lines was calculated with respect to the power-law component without absorption. The results of the fitting procedure are shown in Table 6.

The spectral properties of N and E emission are similar, including $EW_{6.4\ \rm keV}$, which indicates the same origin of the cloud emission. The clump S has the highest flux in the 6.4 keV line and continuum, however its $EW_{6.4\ \rm keV}$ value (570 ± 50 eV) is smaller than for N and E (980 ± 170 eV and 830 ± 200, respectively). From the other side the clump S has the largest size compared to the others. To estimate the surface brightness we divided the observed 2 – 7.5 keV flux of each clump by the corresponding source extraction area as listed in Table 6.

6 DISCUSSION AND SUMMARY

In this paper we present results of a long *NuSTAR* (150 ks) observation of the Arches complex in 2016. The complex includes a stellar cluster with a bright thermal ($kT \sim 2$ keV) X-ray emission and a nearby molecular cloud, characterized by an extended non-thermal X-ray continuum and fluorescent

Table 5. Definitions of the sky regions of the Arches clumps used for the spectral analysis.

Region	RA (J2000)	Dec. (J2000)	Parameters	Area, arcsec^2
Clump S	17:45:52.92	-28:50:21.30	26″, 44″, 130°	3556
Clump N	17:45:49.24	-28:48:54.65	20″, 33″, 169°	1437[1]
Clump E	17:45:52.82	-28:49:25.35	13″, 22″, 162°	906
Excluded cluster	17:45:50.47	-28:49:15.70	16″, 29″, 177°	

[1]) The surface area of clump N is computed with the cluster region excluded.

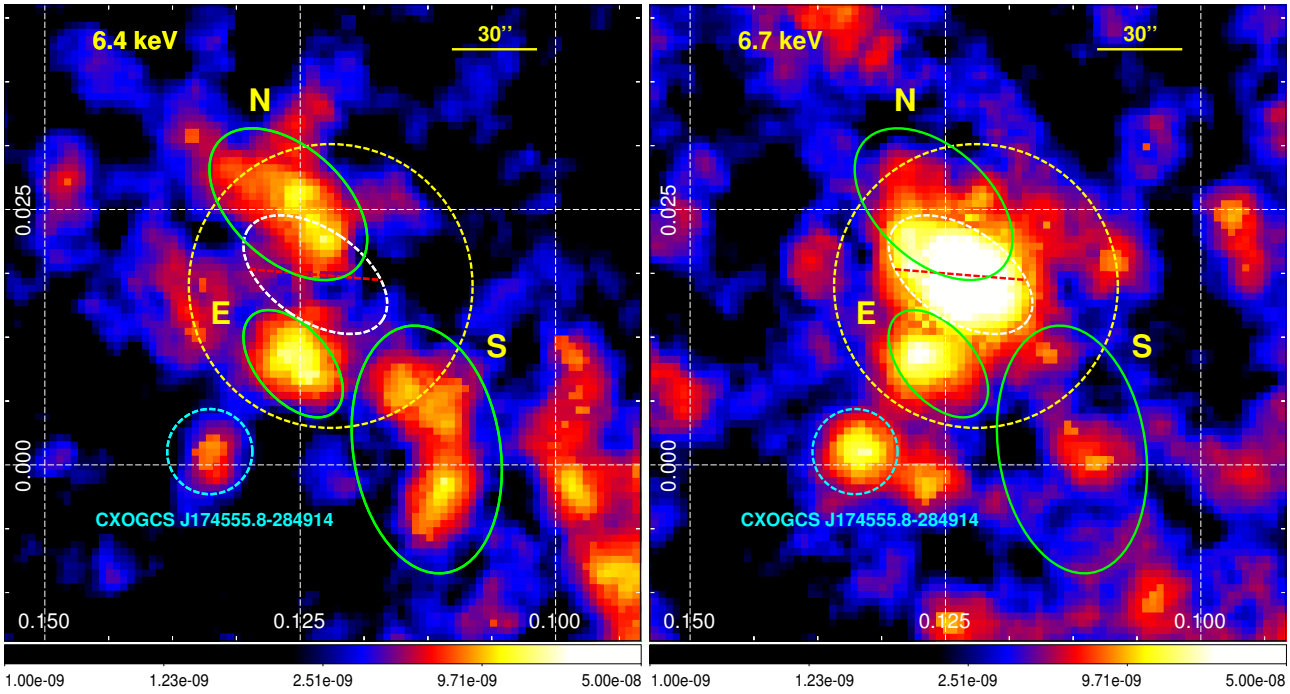


Figure 7. The 6.4 keV (left) and 6.7 keV (right) line flux mosaic images constructed, respectively, in the 6.32 – 6.48 and 6.62 – 6.78 keV energy bands (*XMM–Newton*, 2015, Krivonos et al. 2017). The maps are continuum subtracted and shown in Galactic coordinates. The solid ellipses represent the source spectrum extraction regions of the Arches cloud clumps. The cluster core emission bright in 6.7 keV line is shown by the dashed ellipse. The small dashed circle ($R = 15''$) indicates the position of the hard X-ray source CXOGCS J174555.8–284914 (Yusef-Zadeh et al. 2002; Law & Yusef-Zadeh 2004). The large dashed circle region ($R = 50''$) shows the source spectrum extraction region of the Arches cluster non-thermal emission (see Sect. 2). The images are adaptively smoothed using the DMIMGADAPT task from CIAO-V.4.9 with the following parameters: tophat kernel, smoothing scales 0.1 – 5, the number of scales is 10, the minimum number of counts is 20.

Fe K_α 6.4 keV line. Recent *NuSTAR* and *XMM–Newton* observations of the Arches non-thermal emission demonstrate a dramatic change both in morphology and intensity, and continuous observations are needed to shed light on the nature of the current low-level emission.

Despite the fast decrease observed in 2007-2015 (Krivonos et al. 2017), the *NuSTAR* observations in 2016 show that the non-thermal emission is still present around the Arches stellar cluster, as demonstrated by our spectral and spatial analysis. Furthermore, the 3 – 20 keV flux of the emission in 2016 remains at the same level as measured in 2015 without a significant change in the spectral shape. However, one year interval may not be long enough to see a strong flux variation, which is followed from the fact that the measured 2016 non-thermal flux is not in contradiction with the declining trend observed in 2007-2015 (Krivonos et al. 2017). The overall drop of the $EW_{6.4\ \mathrm{keV}}$ from $\sim$ 0.9 keV in 2002-2015 to 0.6 – 0.7 keV in 2015 (Krivonos et al. 2017) has been confirmed at the same level in 2016. These results may indicate that the intensity of the Arches non-thermal emission reached its stationary level. At the same time, the declining trend predicts the 2016 flux at the level of $F_{3-20\ \mathrm{keV}} = 5.2^{+1.1}_{-0.9} \times 10^{-13}$ erg cm^{-2} s^{-1}, which is consistent within the errors with our measurement $F_{3-20\ \mathrm{keV}} = 4.4^{+2.1}_{-3.1} \times 10^{-13}$ erg cm^{-2} s^{-1} in 2016 (Table 2). Thus, we cannot assess whether the non-thermal emission has reached a stationary level in 2016, and new observations, separated by a longer time period, are needed.

To better constrain the spectral properties of the Arches complex in this state, we constructed its broad-band spectrum using *NuSTAR* 2015-2016 and *XMM–Newton* 2015 observations, with the total exposure time of 350 ks and 114 ks, respectively. The joint fit gives a solid measurement of the power-law $\Gamma = 2.21 \pm 0.15$ up to 30 – 40 keV, which is, how-

Table 6. Best-fitting model parameters of three non-thermal emission clumps around the Arches stellar cluster measured with *XMM–Newton* in 2015. The model is described in XSPEC notation as $wabs \times (APEC + Gaussian^{2.45\ keV} + powerlaw) + Gaussian^{6.4\ keV}$.

Parameter[1)]	Unit	Clump S	Clump N	Clump E
$N_{\rm H}$	10^{22} cm^{-2}	5.5±0.5	7.2±1.0	8.2±1.1
$I_{\rm kT}$	see Sect. 3.2	0.9±0.5	1.7±0.6	1.3±0.5
$E_{2.45\ keV}$	keV	2.45±0.01	2.46±0.03	$2.37^{+0.07}_{-0.05}$
$N_{2.45\ keV}$	10^{-6} ph cm^{-2} s^{-1}	$5.3^{+1.8}_{-1.5}$	$4.3^{+3.0}_{-2.1}$	$4.9^{+4.0}_{-2.8}$
$EW_{2.45\ keV}$	eV	260±40	710±150	1500±400
$E_{6.4\ keV}$	keV	6.39±0.02	6.39±0.03	6.35±0.03
$N_{6.4\ keV}$	10^{-6} ph cm^{-2} s^{-1}	2.6±0.4	1.4±0.3	1.2±0.3
$EW_{6.4\ keV}$	eV	570±50	980±170	830±200
$N^{\rm pow}_{@keV}$	10^{-5} ph keV^{-1} cm^{-2} s^{-1}	9.1±0.8	2.9±0.7	3.0±0.6
$F^{\rm pow}_{2-7.5\ keV}$	10^{-13} erg cm^{-2} s^{-1}	3.35±0.28	$1.08^{+0.25}_{-0.27}$	1.30±0.22
$S^{\rm pow}_{2-7.5\ keV}$	10^{-17} erg cm^{-2} s^{-1} arcsec^{-2}	9.4±0.8	$7.5^{+1.7}_{1.9}$	14.3±2.4
C		1.02±0.05	0.72±0.06	1.1±0.1
$\chi^2/d.o.f.$		1.33/151	1.18/54	1.07/53

[1)] $S^{\rm pow}_{2-7.5\ keV}$ is the flux in the 2 – 7.5 keV band divided on the clump region area. C denotes cross-normalization factor between MOS1/MOS2 and PN data.

ever softer than $\Gamma = 2.03 \pm 0.16$ measured by Krivonos et al. (2017) in 2015 with the same *XMM–Newton* data set.

The rough 2D spatial analysis with *NuSTAR* shows that the morphology of the non-thermal emission in 2016 is still associated with molecular cloud and is not consistent with the possible emission of the stellar cluster.

Finally, we performed the spectral analysis of three bright Fe K_α line emission clumps of the Arches molecular cloud (Krivonos et al. 2017), based on *XMM–Newton* observations in 2015. The analysis showed different $EW_{6.4\ keV}$ values for clumps S (570 ± 50 eV) and N-E (∼ 900 eV). The clump S also demonstrates a weaker interstellar absorption than two others. This finding confirms that the X-ray emission from the molecular cloud is a combination of two components with different origins. The different *EW*s of the iron K_α line may also be produced by the different reflection geometry of the clumps. Chernyshov et al. (2018) favor the scenario of two Sgr A* flaring events, consistent with different 6.4 keV line *EW*s found in this work. This is also in agreement with the studies of other molecular clouds in the CMZ, which imply two Sgr A* flares (Clavel et al. 2013; Terrier et al. 2018; Chuard et al. 2018).

Further monitoring observations of the Arches complex are strongly needed to trace the on-going evolution of the clumps and to confirm the reached stationary level of the non-thermal emission of the whole Arches cloud region.

ACKNOWLEDGMENTS

This work has made use of data from the *NuSTAR* mission, a project led by the California Institute of Technology, managed by the Jet Propulsion Laboratory and funded by NASA, and observations obtained with *XMM–Newton*, an ESA science mission with instruments and contributions directly funded by ESA Member States and NASA. The research has made use of the *NuSTAR* Data Analysis Software jointly developed by the ASI Science Data Center (ASDC, Italy) and the California Institute of Technology. EK and RK acknowledge support from the Russian Basic Research Foundation (grant 16-02-00294). GP acknowledges financial support from the Bundesministerium für Wirtschaft und Technologie/Deutsches Zentrum für Luft- und Raumfahrt (BMWI/DLR, FKZ 50 OR 1812, OR 1715 and OR 1604) and the Max Planck Society. DC is supported by the grant RFBR 18-02-00075.

REFERENCES

Arnaud K. A., 1996, in Jacoby G. H., Barnes J., eds, Astronomical Society of the Pacific Conference Series Vol. 101, Astronomical Data Analysis Software and Systems V. p. 17
Capelli R., Warwick R. S., Cappelluti N., Gillessen S., Predehl P., Porquet D., Czesla S., 2011a, A&A, 525, L2
Capelli R., Warwick R. S., Porquet D., Gillessen S., Predehl P., 2011b, A&A, 530, A38
Chernyshov D. O., Ko C. M., Krivonos R. A., Dogiel V. A., Cheng K. S., 2018, ApJ, 863, 85
Chuard D., et al., 2018, A&A, 610, A34
Churazov E., et al., 1993, ApJ, 407, 752
Churazov E., Khabibullin I., Sunyaev R., Ponti G., 2017a, MNRAS, 465, 45
Churazov E., Khabibullin I., Sunyaev R., Ponti G., 2017b, MNRAS, 471, 3293
Clavel M., Terrier R., Goldwurm A., Morris M. R., Ponti G., Soldi S., Trap G., 2013, A&A, 558, A32
Clavel M., Soldi S., Terrier R., Tatischeff V., Maurin G., Ponti G., Goldwurm A., Decourchelle A., 2014, MNRAS, 443, L129
Cotera A. S., Erickson E. F., Colgan S. W. J., Simpson J. P., Allen D. A., Burton M. G., 1996, ApJ, 461, 750
Dogiel V. A., Chernyshov D. O., Kiselev A. M., Cheng K.-S., 2014, Astroparticle Physics, 54, 33

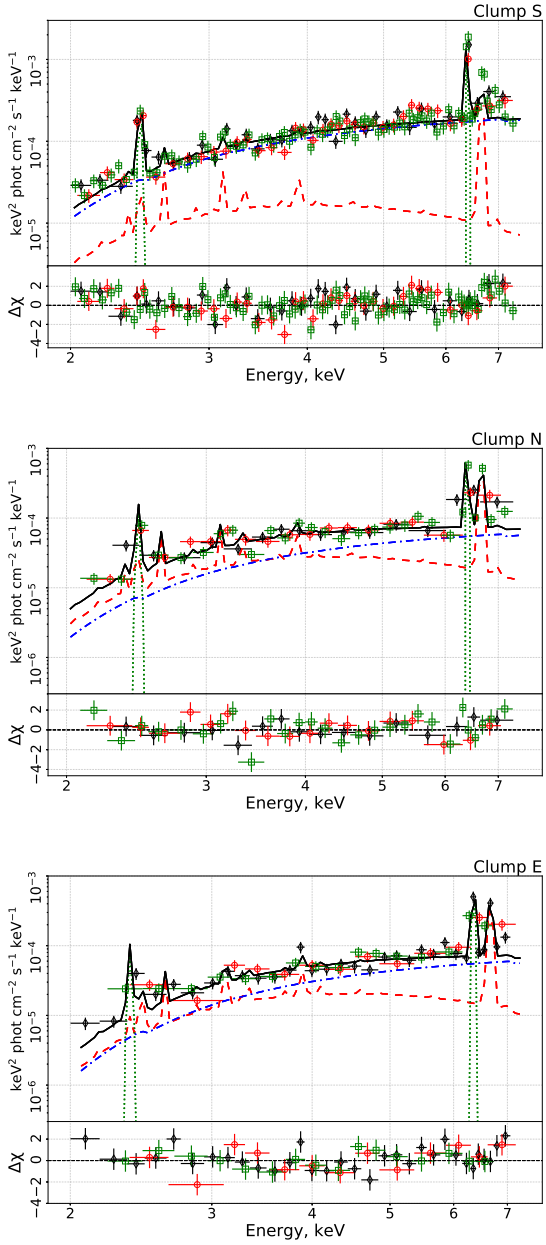


Figure 8. The spectra of each clump obtained with *XMM–Newton* in 2015. Diamonds, circles and squares represent MOS1, MOS2 and PN data, respectively. The spectra were extracted in the 2 – 7.5 keV energy range for all clumps except clump E for which energy range was 2−7.3 keV due to low statistics. The solid line represents best-fit model ($wabs\times(APEC+Gaussian^{2.45\ keV}+powerlaw)+Gaussian^{6.4\ keV}$) with the following components: thermal plasma (dashed), Sulfur 2.45 keV and Fe 6.4 keV line emission (dotted) and non-thermal power-law continuum (dash-dotted).

Figer D. F., Kim S. S., Morris M., Serabyn E., Rich R. M., McLean I. S., 1999, ApJ, 525, 750

Figer D. F., et al., 2002, ApJ, 581, 258

Freeman P., Doe S., Siemiginowska A., 2001, in Starck J.-L., Murtagh F. D., eds, Proc. SPIEVol. 4477, Astronomical Data Analysis. pp 76–87 (arXiv:astro-ph/0108426), doi:10.1117/12.447161

Fruscione A., et al., 2006, in Society of Photo-Optical Instrumentation Engineers (SPIE) Conference Series. p. 62701V, doi:10.1117/12.671760

Harrison F. A., et al., 2013, ApJ, 770, 103

Hong J., et al., 2016, ApJ, 825, 132

Koyama K., Maeda Y., Sonobe T., Takeshima T., Tanaka Y., Yamauchi S., 1996, PASJ, 48, 249

Krivonos R. A., et al., 2014, ApJ, 781, 107

Krivonos R., et al., 2017, MNRAS, 468, 2822

Law C., Yusef-Zadeh F., 2004, The Astrophysical Journal, 611, 858

Madsen K. K., Christensen F. E., Craig W. W., Forster K. W., Grefenstette B. W., Harrison F. A., Miyasaka H., Rana V., 2017, Journal of Astronomical Telescopes, Instruments, and Systems, 3, 3

Mori K., et al., 2015, ApJ, 814, 94

Murakami H., Koyama K., Sakano M., Tsujimoto M., Maeda Y., 2000, ApJ, 534, 283

Ponti G., Terrier R., Goldwurm A., Belanger G., Trap G., 2010, ApJ, 714, 732

Ponti G., Morris M. R., Terrier R., Goldwurm A., 2013, in Torres D. F., Reimer O., eds, Astrophysics and Space Science Proceedings Vol. 34, Cosmic Rays in Star-Forming Environments. p. 331 (arXiv:1210.3034), doi:10.1007/978-3-642-35410-6_26

Revnivtsev M. G., et al., 2004, A&A, 425, L49

Ross R. R., Fabian A. C., 2005, MNRAS, 358, 211

Ryu S. G., Nobukawa M., Nakashima S., Tsuru T. G., Koyama K., Uchiyama H., 2013, PASJ, 65, 33

Serabyn E., Shupe D., Figer D. F., 1998, Nature, 394, 448

Sunyaev R., Churazov E., 1998, MNRAS, 297, 1279

Sunyaev R. A., Markevitch M., Pavlinsky M., 1993, ApJ, 407, 606

Tatischeff V., Decourchelle A., Maurin G., 2012, A&A, 546, A88

Terrier R., et al., 2010, ApJ, 719, 143

Terrier R., Clavel M., Soldi S., Goldwurm A., Ponti G., Morris M. R., Chuard D., 2018, A&A, 612, A102

Tsujimoto M., Hyodo Y., Koyama K., 2007, PASJ, 59, 229

Wang Q. D., Dong H., Lang C., 2006, MNRAS, 371, 38

Wenger M., et al., 2000, A&AS, 143, 9

Yusef-Zadeh F., Law C., Wardle M., Wang Q. D., Fruscione A., Lang C. C., Cotera A., 2002, ApJ, 570, 665

Zhang S., et al., 2015, ApJ, 815, 132

This paper has been typeset from a TEX/LATEX file prepared by the author.